J. Earth Syst. Sci. (2023)132 27
https://doi.org/10.1007/s12040-023-02049-6

The hardgrounds of the Turonian–Coniacian carbonates of the Bagh Group of central India

Dhiren Kumar Ruidas[1,*] and J J P Zijlstra[2]

[1]*Department of Geology, Govt. General Degree College, Manbazar-II, Purulia, India.*
[2]*GeoChemTec, 6445 CJ Brunssum, The Netherlands.*
**Corresponding author. e-mail: dhiren.geol@gmail.com*

MS received 11 March 2022; revised 11 October 2022; accepted 24 October 2022

The Upper Cretaceous of central India is represented by a thin transgressive-regressive succession of tropical marine sediments deposited on a Precambrian basement and covered by massive Deccan Trap basalt flows. At the height of the transgression, a few meters thick succession of very thinly and rhythmically bedded, laterally continuous, muddy carbonates of the Turonian–Coniacian Bagh Group was deposited. The planar to wavy beds consist of nodular to massive limestones intercalating with marls. Eroded, bored, and encrusted hardgrounds occur at regular intervals in succession. Field appearance, results of thin-section petrography, and stable isotope signature of micro-sample carbonates suggest that the hardgrounds formed in a supra- to very shallow sub-tidal, restricted marine environment, which was characterised by repeated emergence and soil genesis. Knowing moments of zero-sea level in a regular rhythmically bedded succession with accurate chronostratigraphy allows for better reconstruction of Indian intracratonic basin dynamics during the Upper Cretaceous and its correlation to global events.

Keywords. Hardground; Bagh Group; isotope; Turonian–Coniacian.

1. Introduction

The Cretaceous global relative sea-level rise caused expansive epeiric seas that formed vast carbonate platforms, preserving signatures of marine transgression and regression (Coimbra *et al.* 2016, 2017; Wilmsen *et al.* 2018; Ruidas *et al.* 2020).

In the eastern Tethyan Region of central India, platform sediments are represented by the Turonian–Coniacian Bagh Group carbonates. They are formed in a (sub)tropical climate at a paleolatitude of about 30°S (Barron *et al.* 1981), supposedly as an eastern arm of the Tethys Sea transgressed through an intracratonic rift basin (Agarwal 1986; Acharyya and Lahiri 1991; Acharyya and Roy 2000; Tripathi 2006; Kumar *et al.* 2018).

The Bagh Group carbonates are shallow marine carbonates like the Red Bar and Rock River deposits of Eastern Wyoming (Jacobs 2020), the late Cretaceous chalk of NW Europe (Voigt 1959; Zijlstra 1995), or the carbonate platforms of the Adriatic (Skelton *et al.* 2003).

This research concerns a detailed investigation of the Bagh Group exposures in the Dhar district of central India (Survey of India toposheet 1:50000, No 8. 46N/3L 46J/15). The ∼10 m thick Bagh Group sediments are well exposed along the

Published online: 04 February 2023

northern flank of the river Narmada near Chakrud, Kasdana, Baria, Mohi, Karondia, Zeerabad, Phutlibaori, Sitapuri, and Rampura (figure 1A, B).

The Bagh Group contains laterally continuous hardgrounds, which are cemented, bored and encrusted layers that formed during times of non-deposition and intense sea bottom lithification (Ruidas *et al.* 2018). They are prominent stratigraphic markers within this overall transgressive succession (Shitole *et al.* 2021). They have been reported elsewhere from deposits of shallow marine environments from the Turonian–Coniacian stages. Moreover, marine hardgrounds may represent the physical expression of pivotal time intervals in Earth's climatic and evolutionary history (Olszewska-Nejbert 2004; Christ *et al.* 2015).

The regular rhythmic bedding of the cemented Bagh Group carbonates suggests earth-orbital forcing of climate that influenced sedimentation rates and early diagenetic lithification. Studying the Bagh Group hardgrounds leads to a better understanding of the relationship between sedimentation rates and early diagenetic lithification of the carbonate sediment. Recognising bed-by-bed

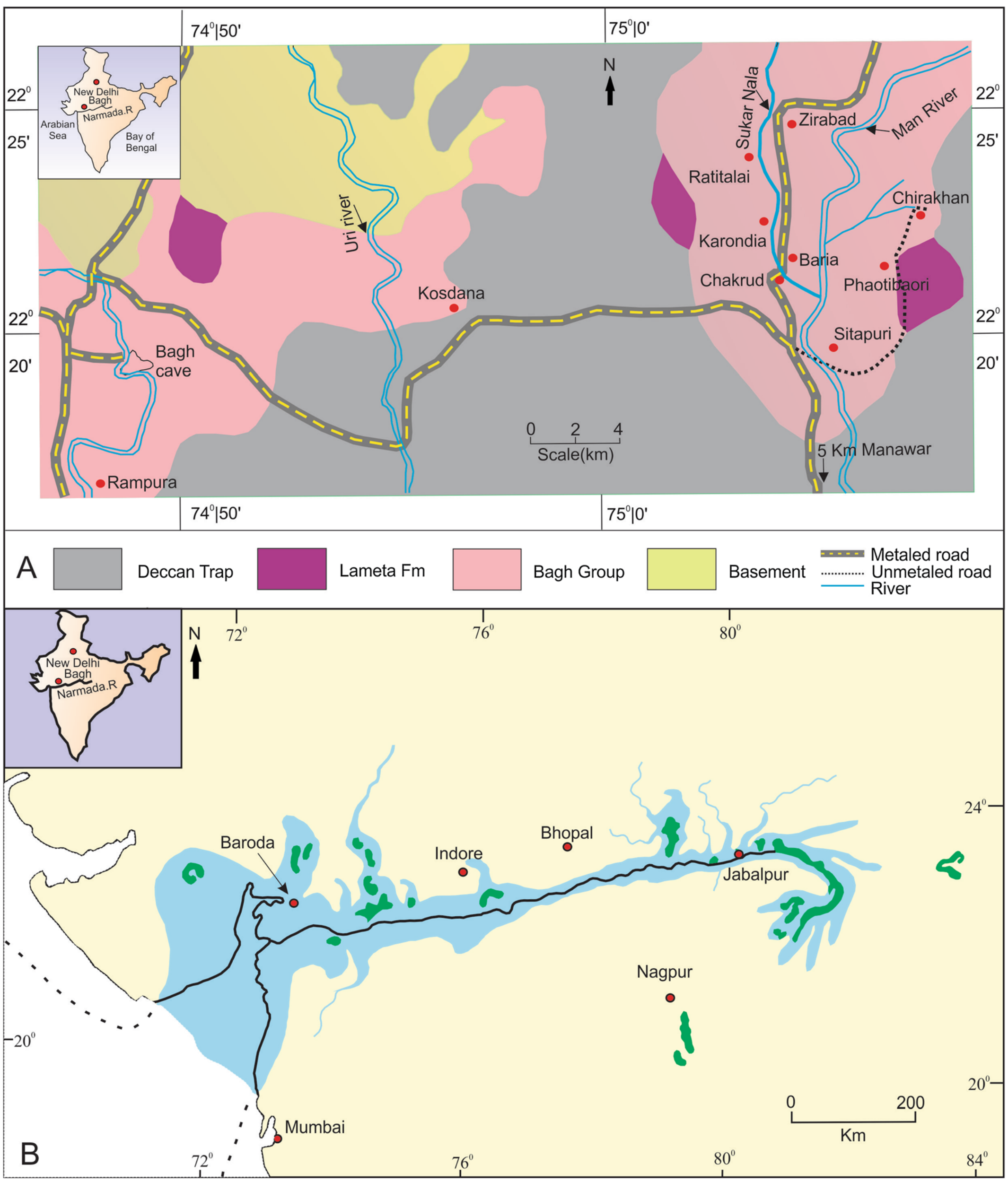

Figure 1. (**A**) Geological map showing outcrops of Bagh Group, Lameta Formation and locations of the study area in central India. (**B**) Paleogeographic map showing outcrops of the Bagh Group in central India during the Late Cretaceous (Turonian) (Singh 1981). Marine palaeo shoreline from west up to Jabalpur and beyond; Green patches are outcrops of Bagh sediments.

variations of sedimentation rate allows for a more detailed reconstruction of chronostratigraphy in support of biostratigraphy, where the hardgrounds provide excellent marker beds that may aid in recognition of eventual hiatus.

The Bagh Group hardgrounds have been investigated in detail, studying field outcrops, identifying petrographic microfacies in thin sections, and analysing stable carbon and oxygen isotope signature of carbonate micro-samples. The results are used to discuss the dynamics of the depositional environment, the timing of the hardground genesis, and the importance of the Bagh Group carbonates for the reconstruction of the Upper Cretaceous paleo-environment.

2. Lithostratigraphy

Within the lithostratigraphy of the Narmada basin (Shitole *et al.* 2021), our investigated composite succession of the Bagh Group (figure 2) shows the Nimar Formation, the Nodular Limestone Formation, and the Bryozoan Limestone Formation (Ruidas *et al.* 2018). The Cenomanian fluvio-marine siliciclastic Nimar Formation rests on the Precambrian crystalline rocks (Sarkar 1973). The siliciclastic deposits are overlain by marine carbonates of the Turonian Nodular Limestone Formation and the Coniacian Bryozoan Limestone Formation. The carbonate deposits are overlain by the Maastrichtian fluvio-marine, siliciclastic Lameta Formation or by flood basalts of the Deccan Traps (i.e., at Chirakhan).

The Nodular Limestone Formation can be further divided into three members (Ruidas *et al.* 2020). The lower wackestone–mudstone member (WMM) varies from three to five meters in thickness, is mainly planar bedded with the colour varying from dark to creamy white and grey to pinkish grey, and with individual bed thickness between 6 and 15 cm. It is essentially a wackestone–mudstone alternation, characterised by a paucity of fossils and a low degree of bioturbation. This lower member ends with a sharp boundary and at Rampura, this horizon occurs between a pink layer below and a few centimetre-thick clay layer above. The middle nodular wackestone member (NWM) is slightly lighter in colour and the beds are more nodular than the lower member. The middle member is rich in invertebrate fossils and is essentially a wackestone. The middle member ends with a planar erosion surface on top of an intensely burrowed layer that developed into a bored hardground. The upper poorly bedded wackestone member (PBWM) is characterised by a distinct nodularity, and it has a high proportion of argillaceous material in the form of relatively thick seams wrapping around the limestone nodules. The upper member is essentially a poorly bedded wackestone, ending with a hardground.

The overlying Bryozoan Limestone Formation (BLF) is more resistant to weathering and forms low ridges in outcrop. It consists of cross-bedded carbonates that locally end in firm- or hardgrounds.

3. Palaeobiogeography

The Tethys Sea of the Late Cretaceous was so wide that the epicontinental faunas of different areas were dissimilar and therefore, many workers preferred to subdivide the Tethyan Realm into faunal provinces (Kennedy *et al.* 2003). The spreading of the seafloor and the concomitant breakup of Gondwanaland created the Indian Ocean influencing the eastern Tethyan Sea during the Late Cretaceous. Characteristic fauna of, especially ammonites, occurs in Madagascar, southern India, and Japan, constituting the Indo-Pacific Faunal Realm sensu Matsumoto (1973). In the Bagh Group, various affinities of ammonite faunas are demonstrated by *Placenticeratidae* and ancillary *Coilopoceratidae*. *Placenticeratidae* from the Coniacian horizons in the Nodular Limestone Formation is represented by a complete population structure, which was also found in Madagascar and Zululand, South Africa. Besides, it also occurs sporadically in Angola and in the Alphard Group of the Cape Province, South Africa (Gangopadhyay and Bardhan 2000). *Coilopoceras* in the Bagh Group was excessively and subjectively split. A thorough systematic revision reveals the presence of only a highly variable dimorphic species of *Coilopoceras*, which was recorded from the base of the Nodular Limestone and was assigned a Middle–Late Turonian age (Kennedy *et al.* 2003).

4. Biostratigraphy

Kennedy *et al.* (2003) reported *Prionocyclus germari* (Reuss 1845), a marker ammonite of the latest Turonian occurring in the Bagh Group. The type species of *Barrosiceras*, i.e., *B. onilahyense* (Basse 1947), having a wide biogeographic distribution

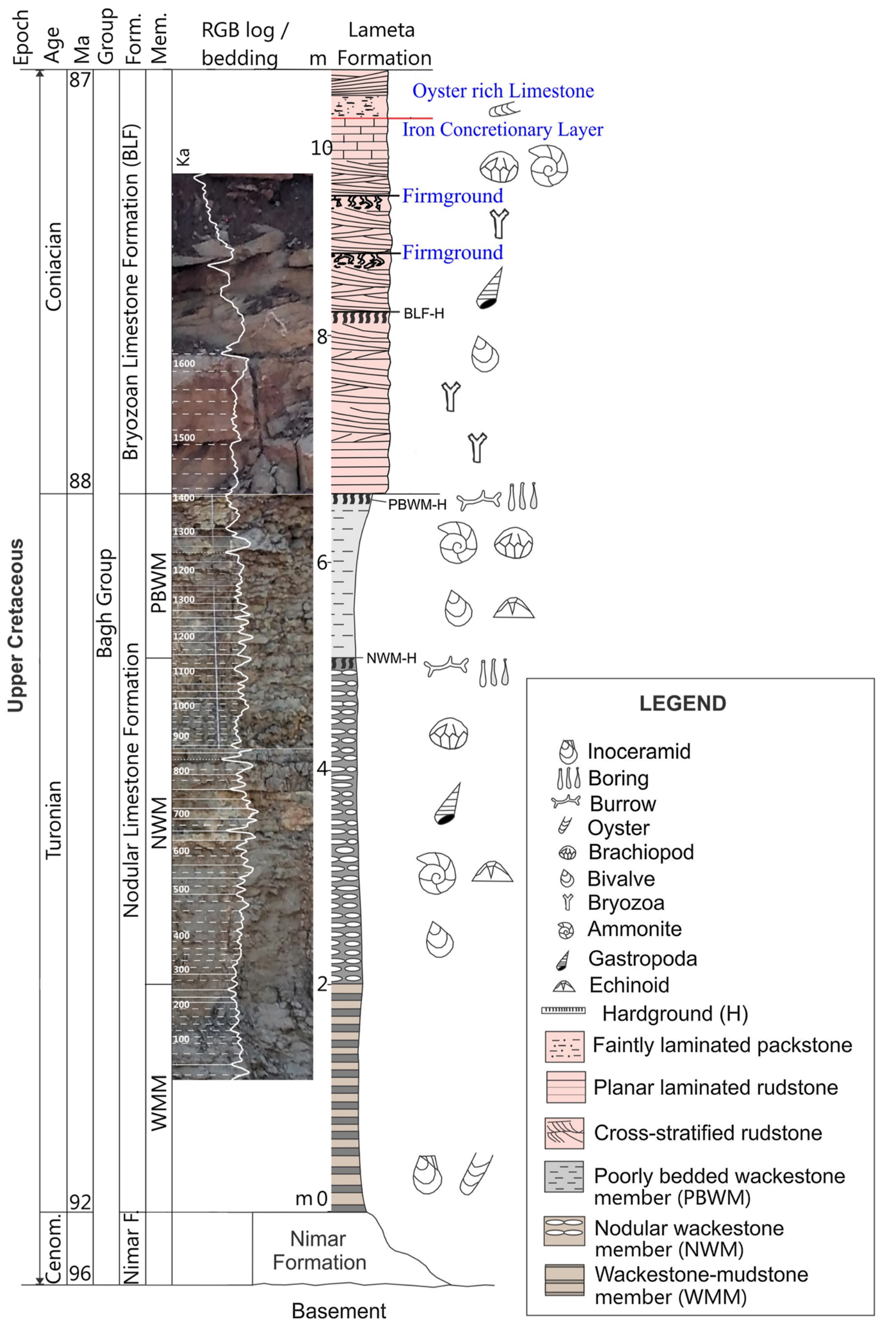

Figure 2. Stratigraphic log of the Bagh Group with detailed log of bedding as exposed in the Ratitalai section, indicated by vertical variation of horizontally averaged pixel colour (red, green, blue) values of darker and lighter layers, and the composite section as exposed around the Manawar area.

cutting across several faunal provinces, is found in the Middle Coniacian beds of the Bagh Group (Gangopadhyay and Bardhan 2000).

Recently, Kumar *et al.* (2018) proposed Cenomanian, Turonian, and Coniacian ages for the Nimar Sandstone Formation, the Nodular Limestone Formation, and the Bryozoan Limestone Formation, respectively (figure 2). Based on the timing of marine transgression and occurrence of the guide fossils ammonite *Placenticeras kaffrarium* (Etheridge 1904) and inoceramid *Volviceramus involutus* (Sowerby 1828), the age of the Nodular Limestone has been refined to Late-Middle or early Late Turonian (Kennedy *et al.* 2003) to Early-Middle Coniacian (Gangopadhyay and Bardhan 2000). The occurrence of Coniacian large inoceramids *Platyceramus mantelli* (de Mercey 1872), at the lower part, and the ammonite *Barroisiceras onilahyense*, at the upper part of the Bryozoan Limestone Formation, respectively, indicate that the Bagh Group sedimentation continued till the end of the Middle Coniacian

(Ganguly and Bardhan 1993). Gangopadhyay and Bardhan (2000) also proposed a Middle Coniacian age for the Bryozoan Limestone based on a new collignoniceratid ammonite. Jaitly and Ajane (2013) reviewed the biostratigraphy and mentioned a Turonian age for the Nodular Limestone Formation and a Coniacian age for the Bryozoan Limestone Formation. Thus, the overall consideration of the biostratigraphic data points to a Turonian to Coniacian age range for the Bagh Group carbonates (figure 2, Ruidas *et al.* 2018).

5. Methodology

A detailed bed-by-bed analysis of exposures of the Bagh Group in the Narmada basin was carried out to prepare a graphic log (figure 2). Around 50 samples were collected from 10 localities around Man River, Zirabad, Chakrud, Ratitalai, Rampura, Karondia, Kosdana, and Phutlibaori (figure 1A).

Petrography of thin sections of samples was examined using a Leica DM 4500P polarising light microscope connected to a Leica DFC420 camera.

Stable carbon and oxygen isotope ratios of the carbonates were measured in the Stable Isotope Laboratory of the Indian Institute of Science Education and Research, Kolkata. Powdered carbonates were obtained from fresh surfaces of micrite and different generations of cement using a micro-drilling device capable of high-resolution milling (Micro-Mill). Approximately 80–100 μg powdered carbonate samples were inserted in glass vials and allowed to react with 100% phosphoric acid at 80°C using a KIEL IV online automatic carbonate preparation device connected to a MAT 253 mass spectrometer in dual inlet mode. A calcite standard (NBS18) and an internal standard (Z-Carrara) were run to monitor the instrumental drift. All stable carbon and oxygen isotope ratios are reported using the delta (δ) notation per mil (‰) relative to the Vienna Pee Dee Belemnite (VPDB). The analytical reproducibility of the standard is ± 0.3‰ (1σ) for δ^{13}C‰ and ± 0.05‰ (1σ) for δ^{18}O‰.

6. Results

6.1 *The hardground between the middle and upper members of the Nodular Limestone Formation*

The first and oldest hardground is well exposed in the Manawar area. It occurs at the top of the middle nodular wackestone member (NWM) and below the upper poorly bedded wackestone member (PBWM). It is characterised by a brownish or pinkish-yellow colour, extremely hard in the Karondia section, and extensively burrowed, bored, and encrusted. Boring and burrows are strongly impregnated by Fe-oxides. The diameter of the borings is 0.5–4.5 mm. Two types of borings are present, *Gastrochaenolites* and *Trypanites* (Taylor and Badve 1995). At Khod–Chikhali, the hardground is glauconitized and bored by *Trypanites*. The vertical sections, as well as bedding planes of the hardground, often exhibit desiccation cracks and root structures. In the Rampura section, the surface is strongly micritised and recrystallised. Dissolution vugs and fissures penetrate perpendicularly, 5–15 cm downwards into the bed. Fossil roots, root moulds, microscopic rhizoliths, and other fabrics characteristic of calcretic soil development, like soil pisoids and mottling of calcrete, are found (figure 3a). Some cavities are filled with sediment containing angular mm- to cm-sized fragments of the host rock and, rarely, yellow to brown marly-clayey material.

Petrographic examination reveals that the borings have been filled by vadose silt consisting of silt- to sand-sized particles in a micritic to microsparitic matrix (figure 3e, f). Bioclasts have been coated by Fe-oxides and are strongly bored. Benthic Foraminiferas are very rare and present inside brachiopods, pelecypods, and gastropods. The frequently bored bioclasts are composed of broken shell fragments and echinoderm skeletal elements. Thin desiccation cracks are very common.

6.2 *The hardground between the Nodular Limestone Formation and the Bryozoan Limestone Formation*

The second hardground occurs at the top of the Nodular Limestone Formation and below the Bryozoan Limestone Formation (figure 4a–d). It is a 20-cm thick layer with a rust-brown coloured surface that is strongly impregnated by Fe-oxides. Bioclasts are frequently bored with echinoderm and bryozoan remains (figure 4f). Burrows of the moderate to intense omission suite (Ruidas *et al.* 2020) are commonly filled with the same sediment as found in the overlying facies. The surface is encrusted with large and small oysters. Some of the

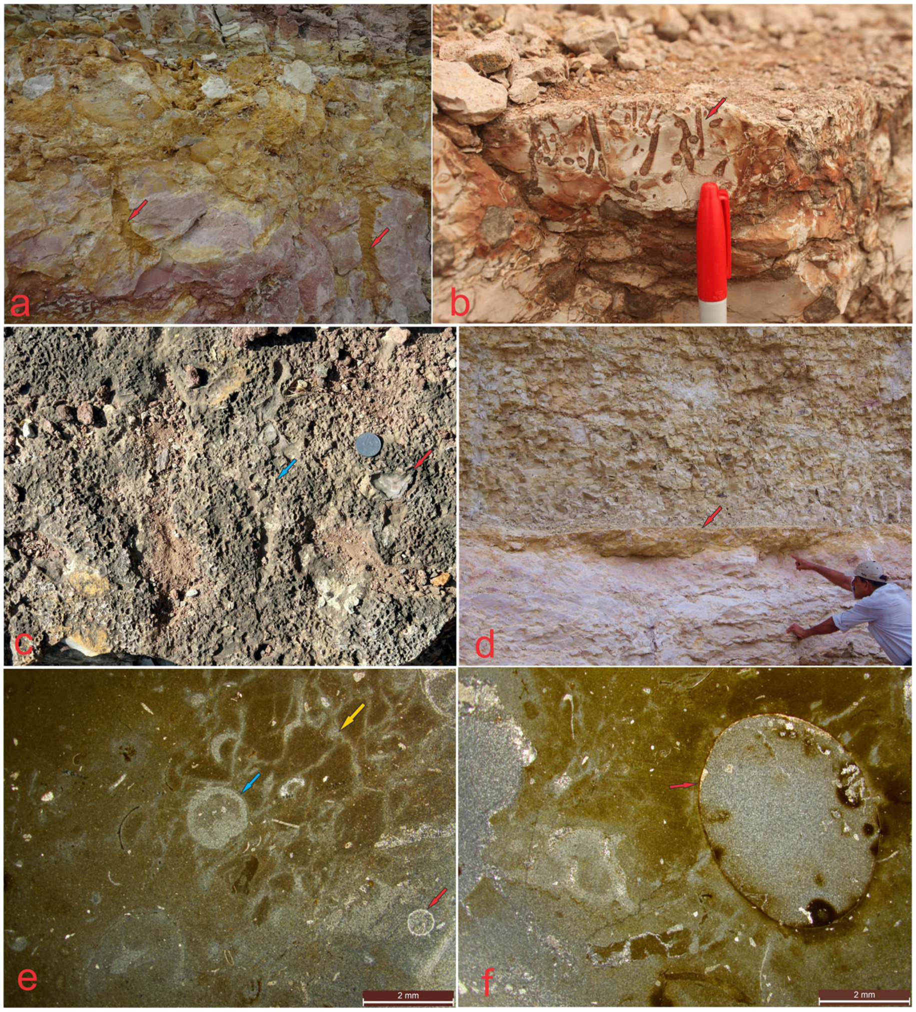

Figure 3. Field photograph showing vertical section of the 1st hardground between middle and upper members of the Nodular Limestone Formation. **(a)** Vertical section of hardground in pedogenic limestones with root structures (arrows); **(b)** borings are strongly impregnated by Fe-oxide (marker pen length = 13 cm); **(c)** plan view showing boring (blue arrow) and encrusting oyster (red arrow) (coin diameter = 2.7 cm); and **(d)** contact between middle and upper nodular limestone members. Photomicroscopic views under plane-polarized light: **(e)** Boring (red arrow), hairy, wavy and bifurcated rootlets (yellow arrow) with micrite coating and boring of bioclasts (blue arrow); and **(f)** ferrugination by various Fe mineralization phases inside, alongside and outside of the boring, where a faintly equidimensional habit of opaque iron mineralization suggests oxidized pyrite.

oysters post-date and others pre-date the Fe mineralisation phase. At Zirabad, the hardground is bored by *Gastrochaenolites*, subsequently eroded and truncated, and encrusted by *Chiplonkarina* and oysters (Taylor and Badve 1995).

Petrographically, this hardground of highly bioturbated carbonate shows bioclasts that are dissolved (figure 4e) and partially filled with micrite. Some vadose silt may occur within the hardground. Brachiopods, pelecypods, gastropods, and rare foraminifera fill the borings that often contain a few fragments of bryozoans. Micrite and bioclasts have been impregnated with Fe-oxides (figure 4g). Ferrugination around a boring is cut across by a root and a desiccation crack (figure 4g).

6.3 *The hardground within the Bryozoan Limestone Formation*

The third hardground is present within the Bryozoan Limestone Formation (figures 5a–d). It occurs at the top of one of the cross-stratified units of bryozoan limestone that higher up in the succession-end with firm grounds. The carbonate is a strongly bioturbated wackestone and locally, a packstone. Thalassinoides are common burrows (figures 5a, 6a–b), filled with yellow to dark-coloured sediment. They consist of vertical or inclined, straight or branched, cylindrical shafts and horizontal tunnels with variable interlacements in Y-shape (figures 5a, 6a–b). The burrows are strongly impregnated by Fe-oxides. The diameter of the burrows ranges from 0.6 to 4.5

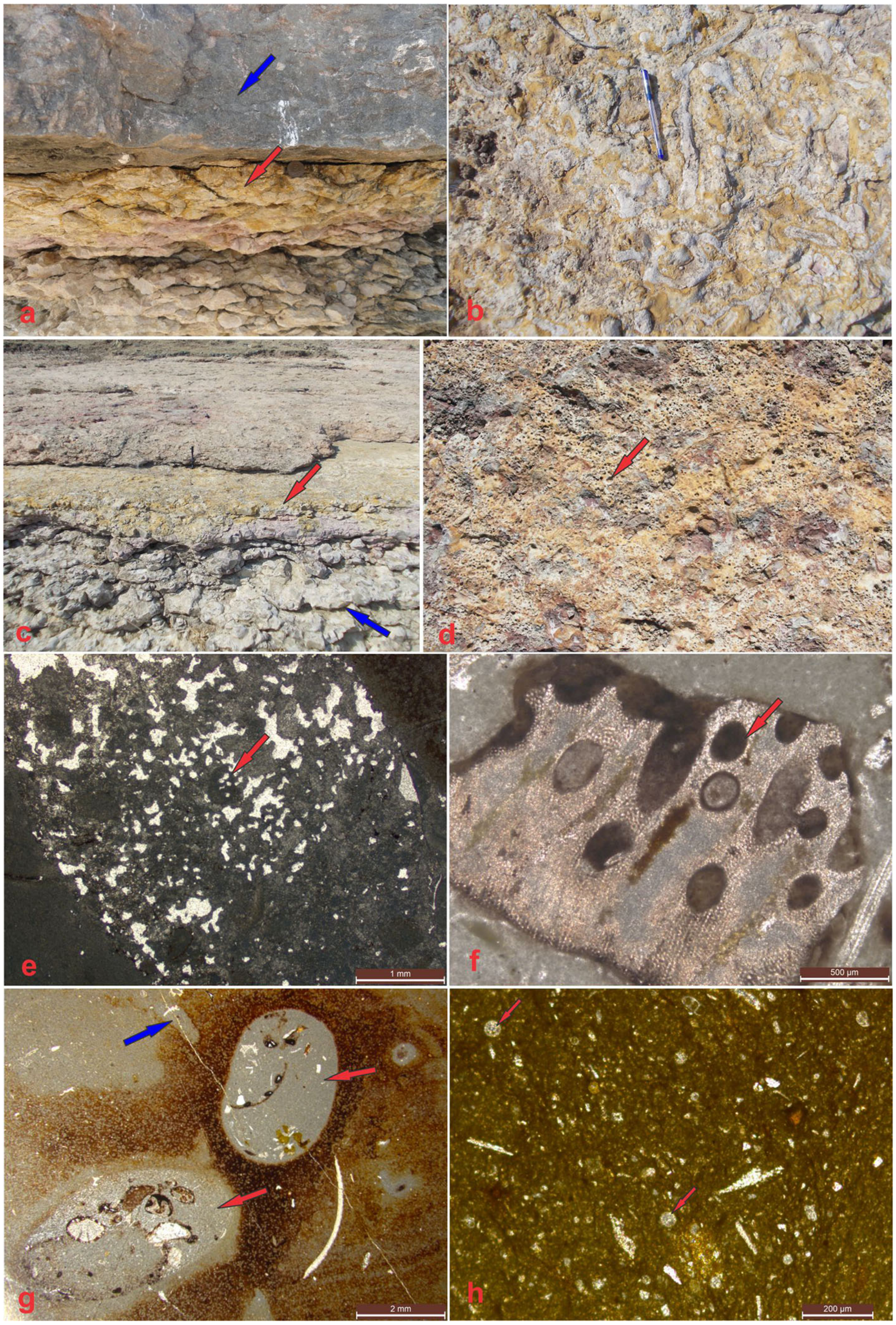

Figure 4. **(a)** Field photograph showing vertical section of 2nd hardground which separates the Nodular Limestone Formation below (red arrow) from the Bryozoan Limestone Formation above (blue arrow); **(b)** plan view showing boring and Thalassinoides burrows (marker pen length = 13 cm); **(c)** vertical section of hardground (red arrow) overlain by bryozoan mat and underlain by nodular limestone (blue arrow); and **(d)** plan view showing boring and Thalassinoides burrows (marker pen length = 13 cm). Photomicroscopic views under plane-polarized light: **(e)** fenestral structures inside of borings; **(f)** intensely bored echinoid fragment with micritization (red arrow); **(g)** Ferrugination around boring cut across by a root and a desiccation crack (blue arrow); and **(h)** boring (red arrow) and surrounding materials.

cm. The burrows are mostly represented by casts, and fragments of shafts are usually characterised by circular cross-sections, while tunnels exhibit oval or ellipsoidal sections depending on host rock lithology.

Post-depositional authigenic minerals are represented by calcite cement and (oxidised) pyrite. Bioclasts are mainly from oysters and bivalves, pebble- to cobble-sized, appearing reworked and partially filling pre-lithification burrows (figure 5d). Numerous *Trypanites* borings occur on the surface of the hardground. The *Trypanites* borings have a somewhat patchy distribution, with

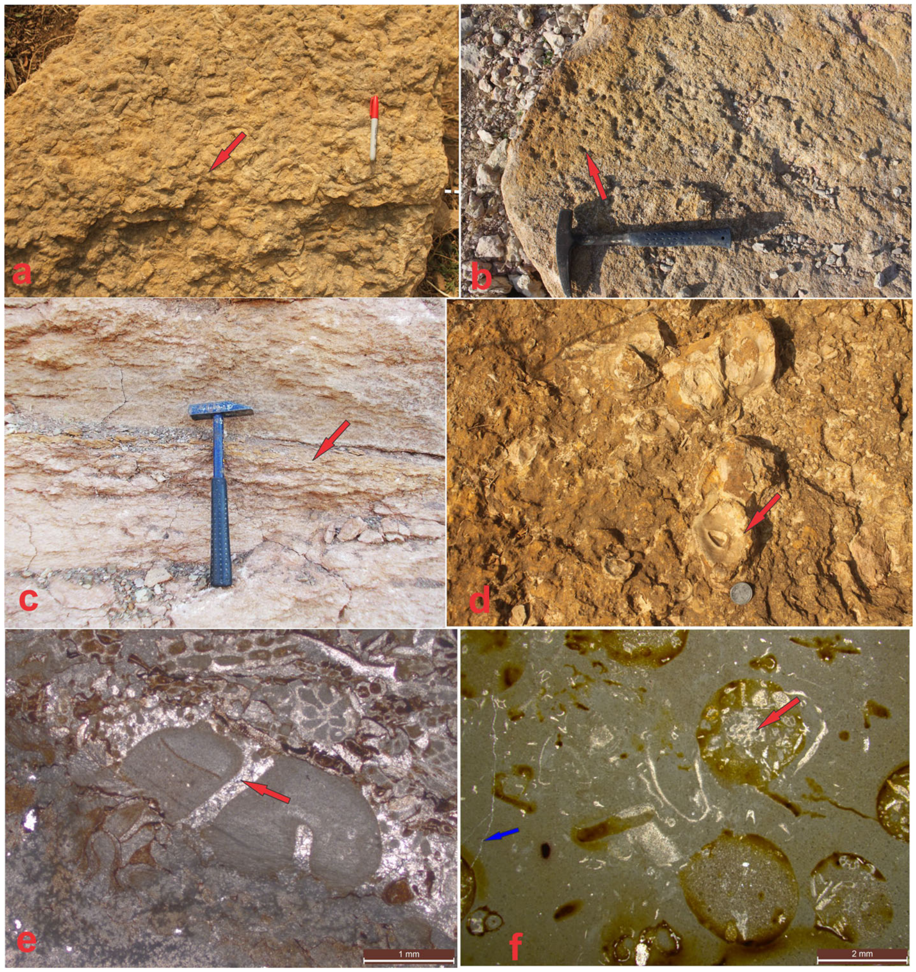

Figure 5. **(a)** Field photograph showing bedding plane of thoroughly bioturbated packstone (pen length = 14 cm); **(b)** plan view showing boring in the hardground (red arrow); **(c)** details of the surface of the hardground in between bryozoan limestones, marked by a red arrow (hammer length = 38 cm); and **(d)** oysters look like pebbles in planar view. Photomicroscopic views under plane-polarized light: **(e)** borings filled by sparite (red arrow) and bryozoan that suffered strong micritization and boring; and **(f)** boring filled by bioclasts (red arrow) and crack filled by sparite (blue arrow).

up to 100 borings counted per 10 cm^2. The diameter of the borings is 0.5–20.4 mm (figure 6c). The apertures are circular, in some cases slightly oval, and the apertures of some borings are merged.

Petrographically, the carbonate of this hardground shows signs of strong bioturbation, and bioclasts are dissolved and partially filled with micrite. Bioclast shell fragments are partly micritised and recrystallised. The fine-grained bioclast-bearing micrite fills about 30% of the volume. Most of the dissolved bioclasts are impregnated/coated by Fe-oxides and are strongly bored (figure 5e–f).

7. Stable carbon and oxygen isotopes

The carbonate isotope signature was measured for samples from the middle (NWM) and upper (PBWM) members of the Nodular Limestone Formation and from the Bryozoan Limestone Formation (BLF). Carbon and oxygen isotopes were measured in the carbonate of the micritic matrix (figure 7) and for the hardgrounds, also in the carbonate of the sparitic cement (table 1; figures 8–10).

The $\delta^{13}C$‰ of the matrix varies between –4 and 2, and it decreases from the lower to the upper units (figure 9). Contemporaneous sequences elsewhere also show a decrease of $\delta^{13}C$‰, however, from about 3 to 1. Hence the Bagh Group matrix carbonates are thus lighter in $\delta^{13}C$‰ (Jarvis *et al.* 2006; Li *et al.* 2006). The $\delta^{18}O$‰ of the matrix varies between –10 and –4, and it also may decrease slightly from lower to upper units (figure 10). Contemporaneous sequences elsewhere show less decrease or even increase from –6 to –5. The Bagh Group matrix carbonates are thus also lighter in $\delta^{18}O$‰.

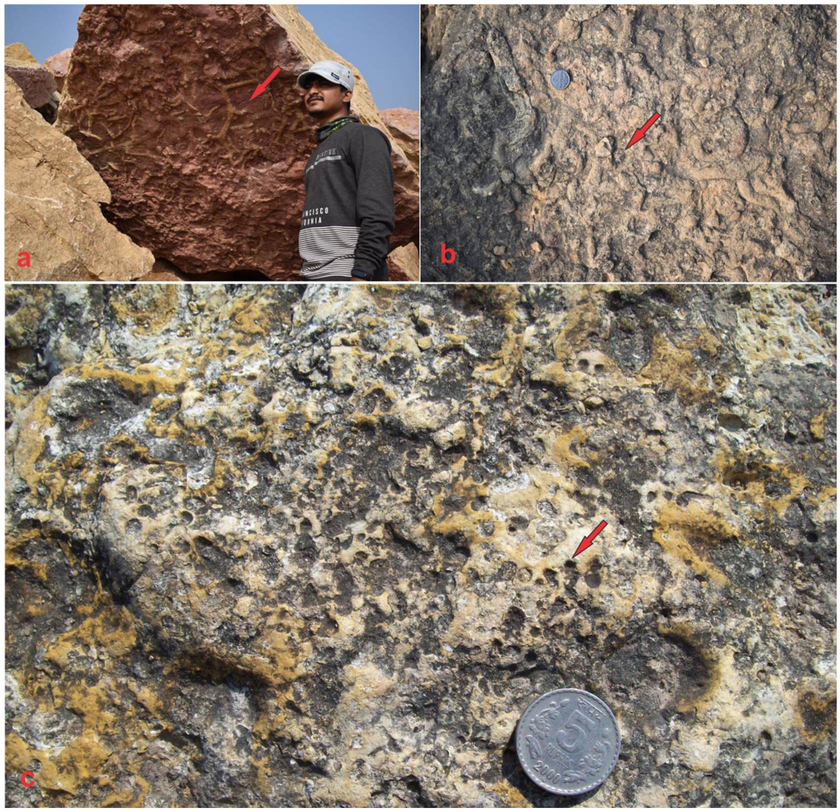

Figure 6. **(a)** Surface of fractured bryozoan limestone running parallel to bedding and showing well-developed Thalassinoides burrows (red arrow) and **(b)** plan view of hardground surface showing bioturbation (red arrow); **(c)** details with many small Trypanites borings (arrow) and few large borings upper right of coin (coin diameter = 2.7 cm).

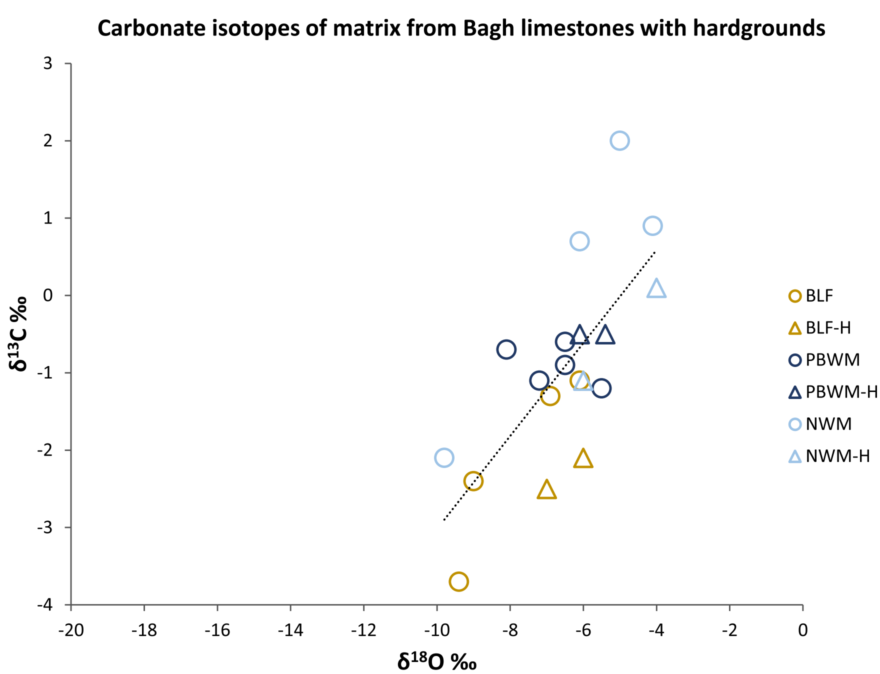

Figure 7. Cross-plot of stable carbon and oxygen isotope ratios of matrix from Bagh Group Limestones with hardgrounds; Nodular Wackestone Member (NWM), Poorly Bedded Wackestone Member (PBWM) and Bryozoan Limestone Formation (BLF), with hardground samples indicated (-H).

Table 1. *Stable isotope signature of Bagh Group micro-samples relative to PDB standard, from Nodular Limestone Formation's middle Nodular Wackestone Member (NWM), upper Poorly Bedded Wackestone Member (PBWM) and Bryozoan Limestone Formation (BLF), with hardground samples indicated (-H) and with distinction of micritic matrix or sparry cement.*

Sample no.	Facies	δ^{18}O‰	δ^{13}C‰	Lithology	Code
BAGH/036	Bryozoan Limestone Formation	–6.1	–1.1	Matrix	BLF
BAGH/035	Bryozoan Limestone Formation	–6.9	–1.3	Matrix	BLF
BAGH/034	Bryozoan Limestone Formation	–9.4	–3.7	Matrix	BLF
BAGH/033	Bryozoan Limestone Formation	–9	–2.4	Matrix	BLF
BAGH/032	Hardground-3	–6	–2.1	Matrix	BLF-H
BAGH/031	Hardground-3	–7	–2.5	Matrix	BLF-H
BAGH/030	Poorly bedded wackestone	–8.1	–0.7	Matrix	PBWM
BAGH/029	Poorly bedded wackestone	–7.2	–1.1	Matrix	PBWM
BAGH/028	Poorly bedded wackestone	–6.5	–0.9	Matrix	PBWM
BAGH/027	Poorly bedded wackestone	–6.5	–0.6	Matrix	PBWM
BAGH/026	Poorly bedded wackestone	–5.5	–1.2	Matrix	PBWM
BAGH/025	Hardground-2	–6.1	–0.5	Matrix	PBWM-H
BAGH/024	Hardground-2	–5.4	–0.5	Matrix	PBWM-H
BAGH/023	Nodular wackestone	–5	2	Matrix	NWM
BAGH/022	Nodular wackestone	–4.1	0.9	Matrix	NWM
BAGH/021	Nodular wackestone	–6.1	0.7	Matrix	NWM
BAGH/020	Nodular wackestone	–9.8	–2.1	Matrix	NWM
BAGH/019	Hardground-1	–6	–1.1	Matrix	NWM-H
BAGH/018	Hardground-1	–4	0.1	Matrix	NWM-H
BAGH/017	Hardground-3	–3.4	–1.1	Cement	BLF-H
BAGH/016	Hardground-3	–9.8	–0.5	Cement	BLF-H
BAGH/015	Hardground-3	–7.5	–2.4	Cement	BLF-H
BAGH/014	Hardground-3	–15.6	–0.9	Cement	BLF-H
BAGH/013	Hardground-3	–8.2	–0.8	Cement	BLF-H
BAGH/012	Hardground-3	–8.2	–3.2	Cement	BLF-H
BAGH/011	Hardground-2	–17.6	–0.9	Cement	PBWM-H
BAGH/010	Hardground-2	–6.3	–0.2	Cement	PBWM-H
BAGH/009	Hardground-2	–9.5	–0.3	Cement	PBWM-H
BAGH/008	Hardground-2	–18.4	–0.6	Cement	PBWM-H
BAGH/007	Hardground-2	–19.1	–0.3	Cement	PBWM-H
BAGH/006	Hardground-1	–18.2	–0.6	Cement	NWM-H
BAGH/005	Hardground-1	–19.1	–0.2	Cement	NWM-H
BAGH/004	Hardground-1	–7.2	–1.7	Cement	NWM-H
BAGH/003	Hardground-1	–7.9	–2.1	Cement	NWM-H
BAGH/002	Hardground-1	–10.7	–1.7	Cement	NWM-H
BAGH/001	Hardground-1	–15	–1.2	Cement	NWM-H
BAGH/036	Hardground-1	–15.5	–1.1	Cement	NWM-H

The stable carbon and oxygen isotope signature of the matrix of hardgrounds and non-hardgrounds is similar (figure 7). The signature of the cement from the hardgrounds allows for a distinction between the two types of cement. Cement with δ^{13}C‰ and δ^{18}O‰ is like that of the matrix and cement with a stable isotope signature that is different from that of the matrix. The latter shows much more negative δ^{18}O‰ down to –20, while the δ^{13}C‰ values tend to concentrate between 0 and –1 as the lighter δ^{13}C‰ values are absent for cement with very negative δ^{18}O‰ (figure 8).

8. Discussion

Although the nodular to massive lithification of the Bagh Group carbonates appear to have been affected by late burial stylolitization (Kahsnitz and Willems 2017) with non-sutured seam solution, deformation, and compression of argillaceous limestone beds (Ruidas *et al.* 2018), the early diagenetic lithification is considered still sufficiently preserved to allow for use in the reconstruction of the depositional environment.

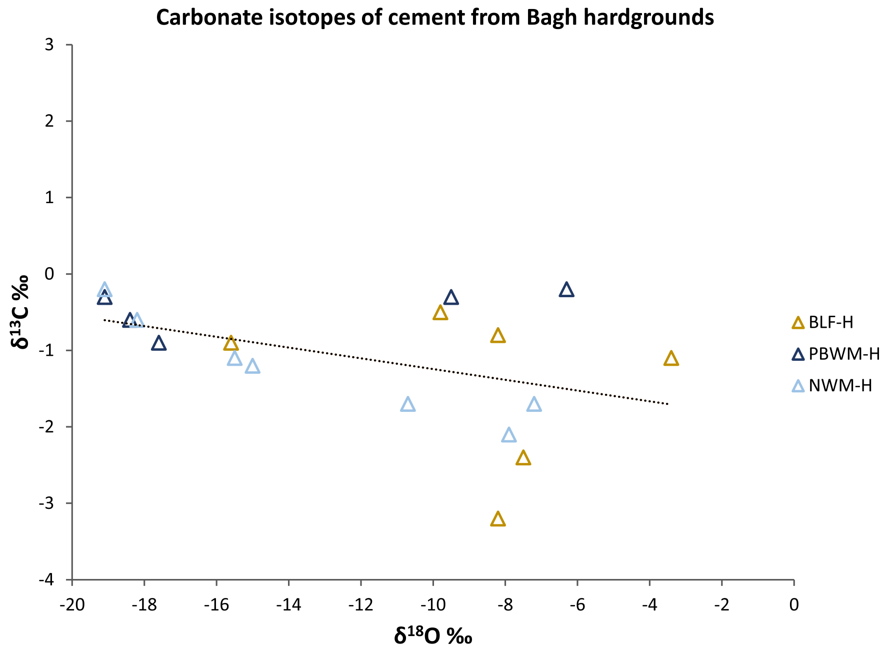

Figure 8. Cross-plot of stable carbon and oxygen isotope ratios of cement from Bagh Group hardgrounds; Nodular Wackestone Member (NWM), Poorly Bedded Wackestone Member (PBWM) and Bryozoan Limestone Formation (BLF), with hardground samples indicated (-H).

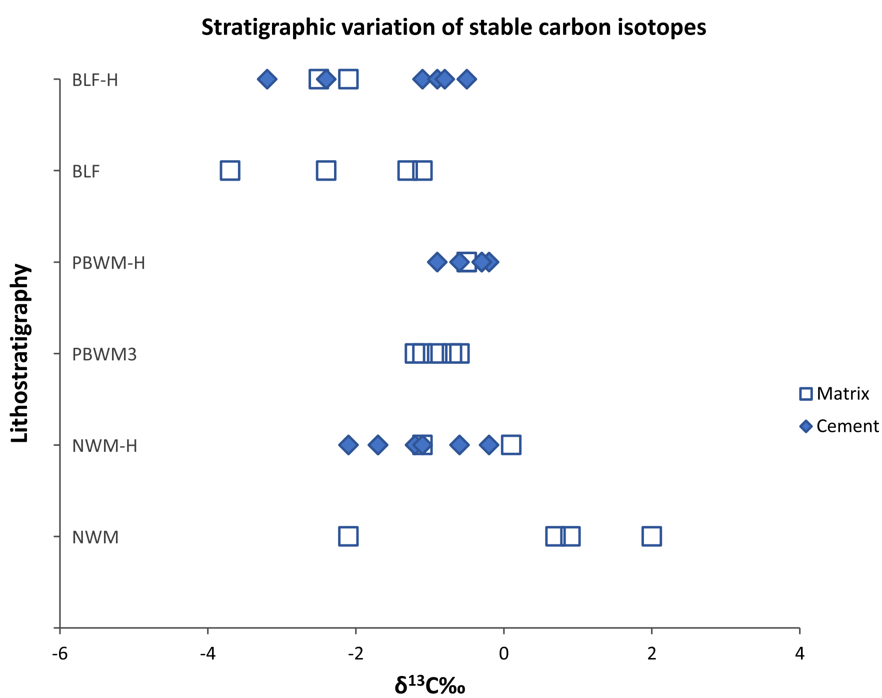

Figure 9. Schematic depiction of the variation of stable carbon isotope values of samples in stratigraphic succession; Nodular Wackestone Member (NWM), Poorly Bedded Wackestone Member (PBWM) and Bryozoan Limestone Formation (BLF), with hardground samples indicated (-H).

8.1 *Environmental reconstruction of the Bagh Group hardgrounds*

Ruidas *et al.* (2020) have argued that the carbonates of the Bagh Group are a transgressive succession of tropical marine sediments deposited in a shallow environment, deepening from predominantly supratidal to intertidal and finally subtidal conditions (figure 11). The changing facies of the successive hardgrounds in the Bagh Group appear to reflect this deepening trend.

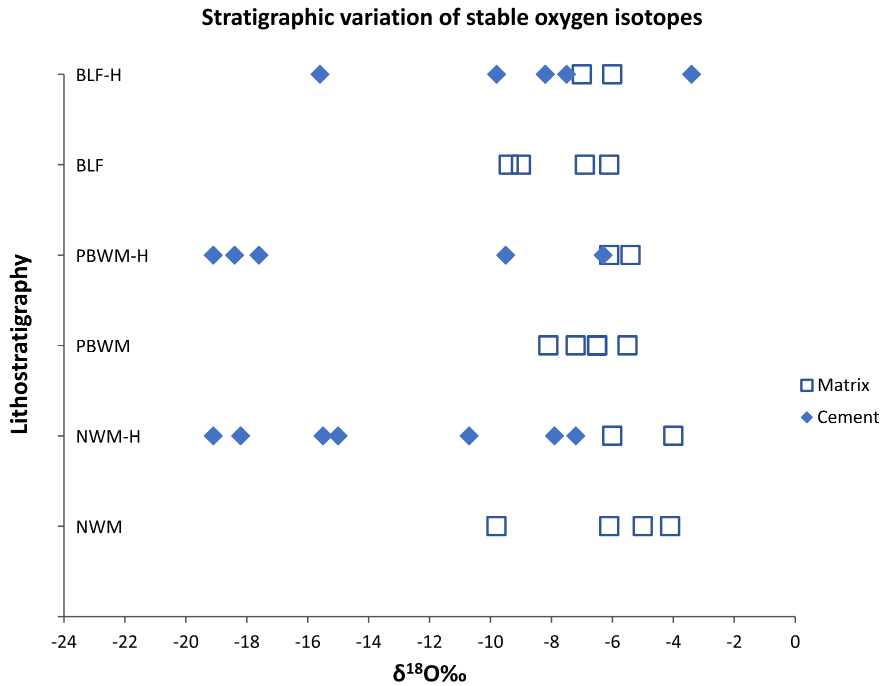

Figure 10. Schematic depiction of the variation of stable oxygen isotope values of samples in stratigraphic succession; Nodular Wackestone Member (NWM), Poorly Bedded Wackestone Member (PBWM) and Bryozoan Limestone Formation (BLF), with hardground samples indicated (-H).

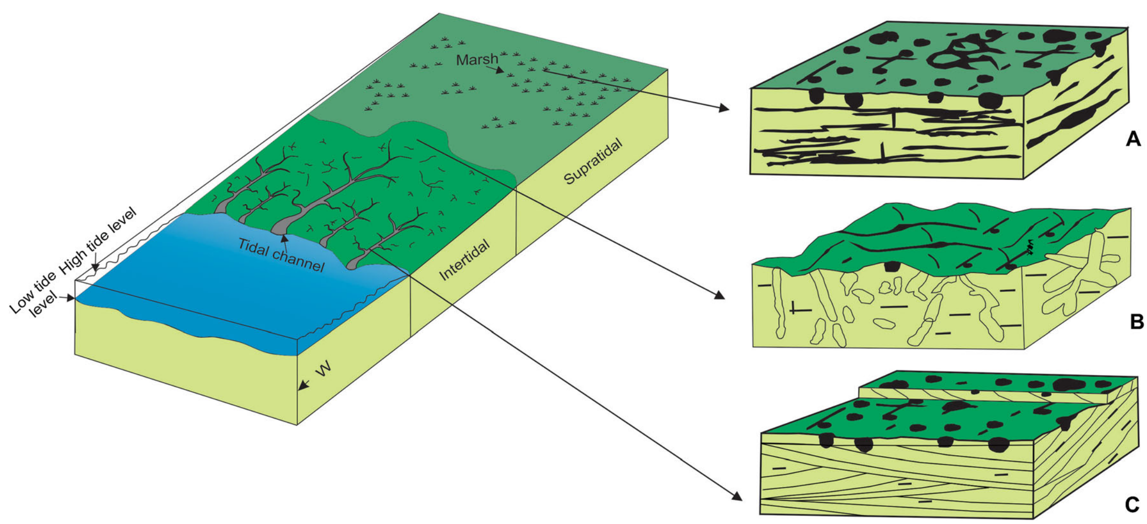

Figure 11. Depositional model showing spatial distribution of hardground surfaces in Bagh Group. Hardground-1 and 2 were deposited in low-energy supratidal to upper intertidal environment **(A, B)**, the hardground-3 formed in the lower intertidal to subtidal environment with tidal channels **(C)** (Ruidas *et al.* 2020).

Carbonate hardgrounds are defined as carbonate seafloors that hardened *in-situ* into firm grounds by the precipitation of carbonate cement in the primary pore spaces and that were subsequently eroded, exposed, encrusted, and bored (Wilson and Palmer 1992; Bodenbender *et al.* 1989; Vinn and Wilson 2010; Vinn and Toom 2015). In the Bagh Group, cyclic variation in cementation and hydrodynamics produced nodular lithification, firm grounds, and three carbonate hardgrounds. Presumably, amongst the various mechanisms proposed for hardground genesis, the lithification of chalk (Kennedy and Garrison 1975) with its typical omission surface ichnofacies (Bromley 1975) seems an appropriate analogue for the genesis of the hardgrounds in the muddy carbonates of the Bagh Group. Shared features are the borings, the overgrowth by

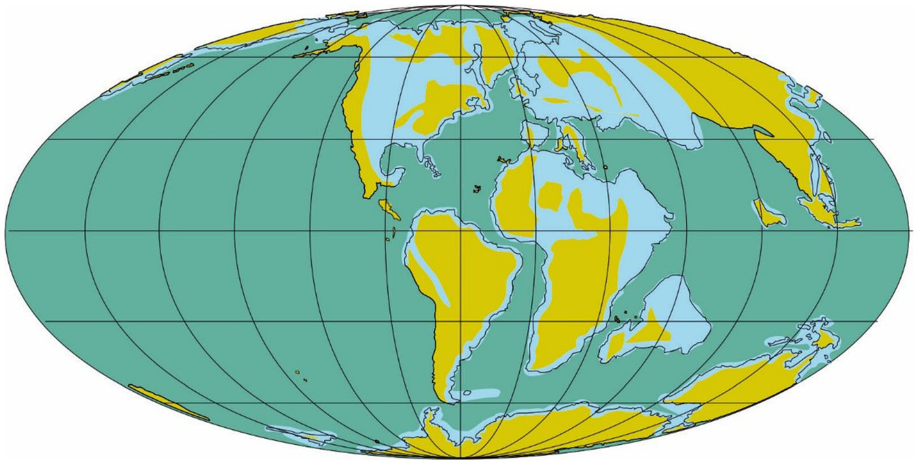

Figure 12. Paleogeographic distribution of Turonian–Coniacian shallow marine environments with hardgrounds (in light blue) (Viviers *et al.* 2000; Delicio *et al.* 2000; Bardhan *et al.* 2002; Piovesan *et al.* 2013, 2014a, b; Puckett *et al.* 2016).

oysters, the micritic nature, the abundance of Bryozoa, the mineralisation by glauconite and pyrite, and the great lateral continuity. Presumably, like the Bagh Group carbonates, the chalk may have been deposited in shallow sub- to supratidal environments (Zijlstra 1997).

The beds of the Bagh Group carbonates are tempestite cycles (Aigner 1982) and formed because of the orbital forcing of climate during precession periods (De Boer and Smith 1994). The hardgrounds formed during precession periods were characterised by an exceptionally strong increase in average storm energy (Zijlstra 1995). This was accompanied by an increasing depth of storm reworking, with the scouring and exposure of carbonates that tend to lithify in anoxic zones of sulphate reduction (Hendry 1993) and methane oxidation at some depth below the fair-weather seafloor surface (Zijlstra 1995; Molenaar and Zijlstra 1997).

The increase in water depth and hydrodynamic energy is relative to that of the preceding cycle. The exceptional decrease of deposition rate, increase of lithification, depth of reworking, exposure of lithified sediment and genesis of hardgrounds may occur simultaneously in the sub, inter-, as well as the supra-tidal environment.

The different Bagh Group hardgrounds may thus have formed under similarly strong relative variations of average water depth and hydrodynamic energy, while the average absolute water depth and hydrodynamic energy were quite different and increased from the supra- to inter- and finally shallow sub-tidal environment, as reflected by properties such as (bioclast) grain size and degree of erosion of the sediment in which mature hardgrounds formed.

The first hardground in the lower part of the transgressive succession, lacking sedimentary structures and with a dominance of micrite, formed in a relatively low-energy depositional environment. The depth of erosion during higher energy conditions was shallow and any sedimentary structures of the thin redeposited storm layers were obliterated by bioturbation. Long periods of subaerial exposure and pedogenesis are indicated by the desiccation cracks, *in-situ* brecciation, micronodulation, calichefication (Calvet and Julia 1983; Flügel and Munnecke 2010; Pomoni-Papaioannou and Zampetakis-Lekkas 2009; Ruidas *et al.* 2020), and vadose silt and root related structures (James and Choquette 1990; Wright 1994; Kraus and Hasiotis 2006). The repeated wetting and subsequent drying by evaporation, lead to dissolution and reprecipitation of the carbonate (Bathurst 1974, 1975; Walker and James 1992; Scholle and Ulmer-Scholle 2003).

During a gradual increase in average storm strength and hydrodynamic energy, deposition decreased and changed into erosion. Presumably, the carbonate sediment of this hardground first lithified at some depth below the seafloor into a firmground, while it experienced prolonged anoxic conditions of sulphate reduction and carbonate cement precipitation (Hendry 1993). Relatively light δ^{13}C‰ values as found in the lithified Bagh Group carbonates have been considered a by-product of sulphate reduction (Dickson *et al.* 2008).

When this layer was subsequently eroded repeatedly and exposed temporarily to be covered again by

Table 2. *List of a selection of Middle–Upper-Cretaceous hardgrounds.*

Sl. no.	Age	Locality	Depositional environment	References
1	Middle-Cretaceous	Northern Neo-Tethys (Turkey)	Continental margin	Eren and Tasli (2002)
2	Upper Cretaceous	Greece	Continental shelf	Pomoni-Papaioannou and Solakius (1991); Pomoni-Papaioannou (1994)
3	Campanian–Maastrichtian	Duwi Formation, Egypt	Shallow-marine	Glenn and Arthur (1990)
4	Campanian–Maastrichtian	Chuangde Formation in Kangmar, southern Tibet of China	Shelf margin	Li *et al.* (2011)
5	Upper Coniacian	Central Jordan		Lewy (1975)
6	Coniacian–Campanian	South and Central Jordan	Pelagic ramp	Powell and Moh'd (2011)
7	Turonian	Bohemian Cretaceous Basin of the Czech Republic	Shallow	Al-Bassam *et al.* (2021)
8	Turonian	Haute Normandie, France		Kennedy and Juignet (1974)
9	Upper Cretaceous	Anglo-Paris Basin (N France)		Jarvis (1980)
10	Middle-Cretaceous	Red Chalk and Lower Chalk (E England)	Continental shelf	Jeans (1980)
11	Upper Cretaceous	Netherlands and Belgium	Continental shelf	Molenaar and Zijlstra (1997)
12	Upper Cretaceous	Mons Basin (Belgium)	Shallow	Richard *et al.* (2005)
13	Upper Cretaceous	Anglo-Paris Basin (S England)	Water depth between 50 and 200–300 m	Kennedy and Garrison (1975)
14	Middle-Cretaceous	Anglo-Paris Basin (SW England)		Garrison *et al.* (1987)
15	Upper Cretaceous	Hole 866A on Resolution Guyot, in the Mid-Pacific Mountains		Arnaud *et al.* (1995)
16	Coniacian	Ivorian Basin	Shallow	Watkins *et al.* (1998)
17	Campanian–Maastrichtian	Maastricht and Kunrade Chalks, Netherlands		Pollock (1976)
18	Middle-Cenomanian	Northern Aquitaine Basin, France		Andrieu *et al.* (2015)
19	Upper Cretaceous	Northern Poland		Leszczyński (2017)
20	Middle and Upper Turonian	Southern England and Northern France		Gale (2019)
21	Upper Cretaceous	Austin Chalk Group of south-central Texas, USA		Cooper *et al.* (2020)
22	Upper Cretaceous	Khasib Formation, Central Mesopotamian Basin, Iraq		Liu *et al.* (2019)
23	Coniacian	Kraków Swell, Poland	Shallow marine	Olszewska-Nejbert and Świerczewska (2013)
24	Coniacian	Wielkanoc quarry, Southern Poland	Shallow marine	Olszewska-Nejbert (2004)
25	Coniacian	NW Europe	Shoreface shallow water	Guinot (2013)

sediment, its surface experienced sub-oxic conditions of iron reduction, causing mineralisation by glauconite and pyrite. Eventually, during times of highest storm strength and hydrodynamic energy conditions, the surface of the firmground became continuously exposed, got encrusted and bored, while reduced iron minerals oxidised to brown iron-oxide upon contact with oxygenated meteoric- or seawater.

A sediment surface that is thus stabilised, lithified, mineralised, and ultimately exposed is prone to rapid colonisation by boring and encrusting endofauna and epifauna, respectively, after drowning by seawater during a subsequent marine incursion (Christ *et al.* 2011).

The second hardground should differ from the first because it occurs higher in the transgressive succession and may have formed at greater water depth and higher hydrodynamic energy than the supratidal hardground below. The fenestral structures are characteristic features of upper intertidal to supratidal environments (Tucker and Wright 1990). However, this hardground below the Bryozoan Limestone Formation also has a well-developed soil-like nature, even more than the first hardground in the Nodular Limestone Formation below. During the precession cycle with exceptional insolation maximum and minimum (Laskar *et al.* 2011), deposition possibly took place in an upper intertidal to supratidal environment. A precession cycle was characterised by, respectively, alternating periods of exceptionally high and low average storm sea levels. During the latter period, prolonged emergence resulted in profound development of paleosol (Martin-Chivelet and Giménez 1992; Gómez-Gras and Alonso-Zarza 2003; Ruidas *et al.* 2020). The abundance of mudstone again indicates a low-energy environment of deposition (Tucker and Wright 1990; Spence and Tucker 1997; Wilson and Evans 2002; Flügel and Munnecke 2010; Fournier *et al.* 2004; Rasser *et al.* 2005; Banerjee *et al.* 2018).

The third hardground formed under the highest-hydrodynamic energy conditions and greatest water depth with the strongest (storm) wave action and with bioclasts that are mostly characteristic of organisms that lived in the lower intertidal to shallow subtidal environment (Ganguly and Halder 1996; Gangopadhyay and Bardhan 2000; Ruidas *et al.* 2020; figure 6). The common *Thalassinoides* burrows suggest a sublittoral to near-shore environment with moderate to high energy conditions (Kumar and Tandon 1979; Singh and Dayal 1979; Singh *et al.* 1983; Kundal and Sanganwar 2000; Srivastava and Mankar 2012; Patel *et al.* 2018). Also, the large-scale wavy bedding, reworked and transported large clasts of lithified sediment, as well as the dense packing and stacking of shells, indicate fluctuating higher water energy conditions.

8.2 *The Bagh Group stable carbon and oxygen isotopes*

The stable δ^{13}C‰ carbon and δ^{18}O‰ oxygen isotope values of the matrix and bioclasts of the Bagh Group limestones (Ruidas *et al.* 2020) are lighter than other marine carbonates of the same age (Jarvis *et al.* 2006; Li *et al.* 2006). They are more like that of Pleistocene Bermuda Limestones (Hudson 1977) and possibly of a secondary origin because of the presence of syn-sedimentary meteoric calcite cement (Saller and Moore 1991). Recrystallisation by meteoric water may also be the cause of the hardground cement with strongly negative δ^{18}O‰ and slightly increased δ^{13}C‰.

The relatively light stable carbon and oxygen isotope signature of the matrix and bioclasts may also have a primary origin, fitting a restricted marine environment that experienced a relatively low open marine influx of heavy isotopes, in contrast to a relatively high influx of light isotopes from photosynthesis and meteoric water precipitation and runoff (Diz *et al.* 2009).

Presumably, the stable carbon and oxygen isotope signature become lighter, moving upward in the stratigraphy of the transgressive succession (figures 9, 10) due to changes in the depositional and early diagenetic conditions. From supra- via inter- to subtidal conditions, an emerged calcretic environment that was dominated by evaporation and decrease of light isotopes changed into a flooded environment dominated by precipitation and increase of light isotopes (Salomons *et al.* 1978).

Further detailed investigation of stable carbon and oxygen isotopes is required to better understand the isotope signature of the Bagh Group carbonates as not only a result of syn-depositional conditions but also of subsequent diagenetic resetting (Christ *et al.* 2015).

8.3 *The Bagh Group hardgrounds in global perspective*

The Cretaceous environment was characterised by a greenhouse climate, warm temperatures, and regular relative sea-level fluctuations (Basilone 2021). Decreased solubility of $CaCO_3$ favoured extensive sedimentation of shallow-water carbonates along the Tethyan margins (figure 12) and facilitated the development of hardgrounds (Taylor and Wilson 2003). Table 2 shows a non-exhaustive list of Middle-Upper Cretaceous hardgrounds and the depth of the depositional environment in which they formed.

At least the formation of the second hardground encountered in the Bagh Group, occurring between the middle Nodular Limestone member with late Turonian *Mytiloides* sp. aff. *labiatoidiformis*

(Tröger) and the upper Nodular Limestone member with Coniacian *Volviceramus* cf. *involutus* (Sowerby, 1828) (Ruidas *et al.* 2018), may coincide with a global event that was responsible for the Turonian–Coniacian biostratigraphic boundary (Reitner *et al.* 1995; Olszewska-Nejbert 2004; Chacón and Martín-Chivelet 2008). The hardground may coincide with a medium cycle boundary of a maximum onlap during a short-term (third order) sea level fluctuation around the Turonian–Coniacian boundary of about 89.9 million years ago (Haq 2014).

8.4 *Chronostratigraphy of the Bagh Group hardgrounds*

The regular, laterally continuous bedding of the Bagh Group carbonates is reminiscent of earth orbitally induced rhythmicity, as it was observed for similar successions elsewhere (Chen *et al.* 2015), allowing for a detailed reconstruction of chronostratigraphy.

Preliminary analysis of outcrop images of nearly 7 m of the middle and upper members of the Nodular Limestone and lower part of the Bryozoan Limestone formations of the Ratitalai section shows that this succession consists of about 80 beds of on average 8.75 cm thickness. The average deposition rate for the 20,000-year precession cycles would have been about 4.4 mm per 1000 years (Ka). The interval would be $\sim$80 $\times$ 20,000 or 1.6 million years in duration. This conforms to the proposed shorter biostratigraphic interval of Middle or Late Turonian to Middle Coniacian for the Bagh Group carbonates (Ruidas *et al.* 2018). This contrasts with the previously proposed longer biostratigraphic interval of the entire Turonian (Taylor and Badve 1995) to middle Coniacian (Gangopadhyay and Bardhan 2000), which is equivalent to a much longer chronostratigraphic interval of about 5 million years (–93.5 to –88.5 Ma). In the latter case, the erosion and genesis of the hardgrounds in the Nodular Limestone and Bryozoan Limestone formations might represent considerable hiatus.

A detailed study of the bedding in correlated outcrops is needed to shed more light on the chronostratigraphy of the Bagh Group carbonates, so that the eventual hiatuses are better defined and the interplay of rhythmically varying cementation and deposition rates as a function of cyclic climate variations, transgressive–regressive movements and longer-term basin dynamics can be better understood.

9. Conclusion

The Turonian–Coniacian Bagh Group carbonates are part of an upper Cretaceous, tropical, shallow marine, transgressive-regressive succession, representing a deepening from supra- to shallow subtidal depositional conditions. The regular rhythmic bedding is defined by carbonate nodules that form below the seafloor. Eventually, they amalgamated into firm grounds. When eroded and exposed, they evolved into bored and encrusted hardgrounds. The hardgrounds occur at regular intervals throughout the transgressive succession and are formed during periods of exceptional relative increase of average water depth and hydrodynamic energy. This was accompanied by relatively deep storm reworking, non-deposition, intensified carbonate cementation and soil genesis. The stable carbon and oxygen isotope signature reflects the transgressive nature of the Bagh Group carbonates and the change from evaporation- to precipitation-dominated, supra- to subtidal environment, respectively. The Bagh Group carbonates might have been deposited at relatively low average deposition rates. The thin beds remind us of precession cycles, inviting the precise chronostratigraphic reconstruction of Indian intracratonic basin dynamics. This contributes to a better understanding of global events during the upper Cretaceous.

Acknowledgements

Authors are thankful to IIT Bombay, GGDC Manbazar-II and universities for infrastructure facilities. The authors thank Santanu Banerjee, Tapas Kumar Gangopadhyay, and Prasanta Sanyal of IISER Kolkata for the stable isotope analysis. We thank Paul D Taylor, Asit K Guha, and anonymous reviewers for their constructive comments on the manuscript.

Author statement

The manuscript is a joint effort of Dhiren Ruidas and Hans Zijlstra. Dhiren: Conceived the idea, performed the fieldwork, provided photographs, gathered the data and prepared the first version of the manuscript. Hans: Analysed images for bedding, modified figure 2, and prepared the four graphs of isotope data.

References

Acharya S K and Lahiri T C 1991 Cretaceous palaeogeography of Indian subcontinent: A review; *Cret. Res.* **12** 3–26.

Acharyya S K and Roy A 2000 Tectonothermal history of the central Indian tectonic zone and reactivation of major faults/shear zones; *J. Geol. Soc. India* **55** 239–256, http://www.geosocindia.org/index.php/jgsi/article/view/69407.

Agarwal C 1986 Structure and tectonics of exposed Tertiary rocks between Narmada and Kim rivers in south Gujarat; *J. Geol. Soc. India* **27**(**6**) 531–542, http://www.geosocindia.org/index.php/jgsi/article/view/65923.

Aigner T 1982 Calcareous tempestites: Storm-dominated stratification in Upper Muschelkalk Limestones (Middle Trias, SW-Germany); In: *Cyclic and Event Stratification*; Springer, Berlin, Heidelberg, pp. 180–198.

Al Bassam K, Rambousek P and Čech S 2021 REE-Rich Turonian Phosphates in the Bohemian Cretaceous Basin, Czech Republic: Assessment as source of critical elements and implications for future exploration; *Minerals* **11(3)** 246.

Andrieu S, Brigaud B, Rabourg T and Noret A 2015 The Mid-Cenomanian Event in shallow marine environments: Influence on carbonate producers and depositional sequences (northern Aquitaine Basin, France); *Cret. Res.* **56** 587–607, https://doi.org/10.1016/j.cretres.2015.06.018.

Arnaud H M, Flood P G and Strasser A 1995 Resolution Guyot (Hole 866A, Mid-Pacific Mountains): Facies evolution and sequence stratigraphy: Northwest Pacific atolls and guyots; In: *Proceedings of the Ocean Drilling Program: Scientific Results* **142** 133.

Banerjee S, Khanolkar S and Saraswati P K 2018 Facies and depositional settings of the Middle Eocene-Oligocene carbonates in Kutch; *Geodyn. Acta* **30** 119–136.

Bardhan S, Gangopadhay T K and Mandal U 2002 How far did India drift during the Late Cretaceous? – Placenticeras Kaffrarium Etheridge, 1904 Ammonoidea used as a measuring tape; *Sedim. Geol.* **147** 193–217.

Barron E J, Harrison C G A, Harrison J L and Sloan Hay W W 1981 Paleogeography: 180 Million Years Ago to the Present; *Eclogae Geologicae Helvetiae* **74(2)** 443–470.

Basilone L 2021 Valanginian cold/warm climatic oscillation and synsedimentary tectonic interaction for drowning the carbonate platform of Southern Tethys (Sicily); *Sedim. Geol.* **423** 105–991.

Basse É 1947 *Les peuplements malgaches de Barroisiceras: Révision du genre Barroisiceras de Gross*; Masson.

Bathurst R G C 1974 Marine diagenesis of shallow water calcium carbonate sediments; *Annu. Rev. Earth Planet. Sci.* **2** 257–274.

Bathurst R G C 1975 *Carbonate sediments and their diagenesis*; Elsevier.

Bodenbender B E, Wilson M A and Palmer T J 1989 Paleoecology of Sphenothallus on an Upper Ordovician hardground; *Lethaia* **22(2)** 217–225.

Bromley R G 1975 *Trace fossils at omission surfaces; The Study of Trace Fossils*; Springer, Berlin, Heidelberg, pp. 399–428.

Calvet F and Julia R 1983 Pisoids in the caliche profiles of Tarragona NE Spain; In: *Coated Grains*; Springer-Verlag, Berlin, pp. 456–473.

Chacón B and Martín-Chivelet J 2008 Stratigraphy of Palaeocene phosphate pelagic stromatolites (Prebetic Zone, SE Spain); *Facies* **54(3)** 361–376.

Chen X, Wang C, Wu H, Kuhnt W, Jia J, Holbourn A and Ma C 2015 Orbitally forced sea-level changes in the upper Turonian–lower Coniacian of the Tethyan Himalaya, southern Tibet; *Cret. Res.* **56** 691–701.

Christ N, Immenhauser A, Amour F, Mutti M, Tomás S, Agar S M, Alway R and Kabiri L 2011 Characterisation and interpretation of discontinuity surfaces in a Jurassic ramp setting (High Atlas, Morocco); *Sedimentology* **59(1)** 249–290.

Christ N, Immenhauser A, Wood R A, Darwich K and Niedermayr A 2015 Petrography and environmental controls on the formation of Phanerozoic marine carbonate hardgrounds; *Earth-Sci. Rev.* **151** 176–226.

Coimbra R, Azerêdo A C, Cabral M C and Immenhauser A 2016 Palaeoenvironmental analysis of mid-Cretaceous coastal lagoonal deposits (Lusitanian Basin, W Portugal); *Palaeogeogr. Palaeoclimatol. Palaeoecol.* **446** 308–325.

Coimbra R, Horikx M, Huck S, Heimhofer U, Immenhauser A, Rocha F, Dinis J and Duarte L V 2017 Statistical evaluation of elemental concentrations in shallow-marine deposits (Cretaceous, Lusitanian Basin); *Mar. Pet. Geol.* **86** 1029–1046.

Cooper J R, Godet A and Pope M C 2020 Tectonic and eustatic impact on depositional features in the upper Cretaceous Austin Chalk Group of south-central Texas, USA; *Sedim. Geol.* **401** 105–632.

De Boer P L and Smith D G 1994 Orbital forcing and cyclic sequences; *Spec. Publ. Int. Assoc. Sediment.* **19** 1–14.

Delicio M P, Coimbra J C and Carreño A L 2000 Cretaceous marine Ostracodafrom the Potiguar basin, northeastern Brazil; *Neues jahrbuch für Geologieund Paläontologie Abhandlungen*, pp. 321–345.

Dickson J A D, Wood R A, Bu Al Rougha H and Shebl H 2008 Sulphate reduction associated with hardgrounds: Lithification afterburn; *Sedim. Geol.* **205(1–2)** 34–39.

Diz P, Jorissen F J, Reichart G J, Poulain C, Dehairs F, Leorri E and Paulet Y M 2009 Interpretation of benthic foraminiferal stable isotopes in subtidal estuarine environments; *Biogeosci.* **6(11)** 2549–2560.

Eren M and Tasli K 2002 Kilop cretaceous hardground (Kale, Gümüshane, NE Turkey): Description and origin; *J. Asian Earth Sci.* **20(5)** 433–448.

Etheridge R 1904 Cretaceous fossils of Natal. 1. The Umkwelane Hill Deposit. *Second report of the Geological Survey of Natal and Zululand*, pp. 69–93.

Flügel E and Munnecke A 2010 *Microfacies of Carbonate Rocks: Analysis Interpretation and Application*; Springer-Verlag, Berlin, https://doi.org/10.1007/10.1007/978-3-642-03796-2.

Fournier F, Montaggioni L F and Borgomano J 2004 Paleoenvironments and high-frequency cyclicity in the Cenozoic south-east Asian shallow-water carbonates: A case study from the Oligo-Miocene buildups of Malampaya (offshore Palawan, Philippines); *Mar. Pet. Geol.* **21** 1–22.

Gale A 2019 Correlation, age and significance of Turonian Chalk hardgrounds in southern England and northern France: The roles of tectonics, eustasy, erosion and condensation; *Cret. Res.* **103** 104–164.

Gangopadhyay T K and Bardhan S 2000 Dimorphism and a new record of Barroisiceras De Grossouvre Ammonoidea from the Coniacian of Bagh, central India; *Can. J. Earth Sci.* **37** 1377–1387.

Ganguly T K and Halder K 1996 Significance of the first record of notiloid from the Upper Cretaceous Bagh group of rocks; *Curr. Sci.* 462–465.

Ganguly T K and Bardhan S 1993 Dimorphism in Placenticerasmintoi from the Upper Cretaceous Bagh Beds, Central India; *Cret. Res.* **14** 747–756.

Garrison R E, Kennedy W J and Palmer T J 1987 Early Lithification and Hardgrounds in Upper Albian and Cenomanian Calcarenites, Southwest England; *Cret. Res.* **8** 103–140.

Glenn C R and Arthur M A 1990 Anatomy and origin of a Cretaceous phosphorite-greensand giant, Egypt; *Sedimentology* **37(1)** 123–154.

Gómez-Gras D and Alonso-Zarza A M 2003 Reworked calcretes: Their significance in the reconstruction of alluvial sequences (Permian and Triassic, Minorca, Balearic Islands, Spain); *Sedim. Geol.* **158(3–4)** 299–319.

Guinot G 2013 Late Cretaceous elasmobranch palaeoecology in NW Europe; *Palaeogeogr. Palaeoclimatol. Palaeoecol.* **388** 23–41.

Haq B U 2014 Cretaceous eustasy revisited; *Glob. Planet. Change* **113** 44–58.

Hendry J P 1993 Calcite cementation during bacterial manganese, iron and sulphate reduction in Jurassic shallow marine carbonates; *Sedimentology* **40(1)** 87–106.

Hudson J D 1977 Stable isotopes and limestone lithification; *J. Geol. Soc. Lond.* **133** 637–660.

Jacobs M 2020 Tectonostratigraphy of the Cenomanian–Turonian Frontier Formation during orogenesis in the greater Green River Basin, Wyoming (Doctoral dissertation).

Jaitly A K and Ajane R 2013 Comments on Placenticeras mintoi (Vredenburg 1906) from the Bagh beds (late cretaceous), Central India with special reference to Turonian nodular limestone horizon; *J. Geol. Soc. India* **81(4)** 565–574.

James N P and Choquette P W 1990 Limestones the meteoric diagenetic environment, Diagenesis; *Geosci. Can. Repr. Ser.* **4** 35–73.

Jarvis I 1980 Geochemistry of phosphatic chalks and hardgrounds from the Santonian to early Campanian (Cretaceous) of northern France; *J. Geol. Soc.* **137(6)** 705–721.

Jarvis I, Gale A S, Jenkyns H C and Pearce M A 2006 Secular variation in Late Cretaceous carbon isotopes: A new d13C carbonate reference curve for the Cenomanian-Campanian (99.6e70.6 Ma); *Geol. Mag.* **143** 561–608.

Jeans C V 1980 Early submarine lithifications are common in the Albian and Cenomanian Red Chalk and Lower Chalk of eastern England; *Proc. Yorks. Geol. Soc.* **43** 81–157.

Kahsnitz M M and Willems H 2017 Genesis of Paleocene and Lower Eocene shallow-water nodular limestone of South Tibet (China); *Carbonates Evaporites* **34** 199–218.

Kennedy W J and Garrison R E 1975 Morphology and genesis of nodular chalks and hardgrounds in the Upper Cretaceous of southern England; *Sedimentology* **22(3)** 311–386.

Kennedy W J and Juignet P 1974 Carbonate banks and slump beds in the Upper Cretaceous (Upper Turonian-Santonian) of Haute Normandie, France; *Sedimentology* **21** 1–42.

Kennedy W J, Phansalkar V G and Walaszczyk I 2003 *Prionocyclusgermari* (Reuss 1845), a Late Turonian marker fossil from the Bagh Beds of central India; *Cretaceous* **24** 433–438.

Kraus M J and Hasiotis S T 2006 Significance of different modes of rhizolith preservation to interpreting paleoenvironmental and paleohydrologic settings: Examples from Paleogene paleosols, bighorn basin, Wyoming, USA; *J. Sedim. Res.* **76** 633–646.

Kumar S and Tandon K K 1979 Trace fossils and environment of deposition of the sedimentary succession of Jabalpur, MP; *J. Geol. Soc. India* **20** 103–106, http://www.geosocindia.org/index.php/jgsi/article/view/64525.

Kumar S, Pathak D B, Pandey B, Jaitly A K and Gautam J P 2018 The age of the Nodular Limestone Formation (Late Cretaceous), Narmada Basin, central India; *J. Earth Syst. Sci.* **127** 109.

Kundal P and Sanganwar B N 2000 Ichnofossils from Nimar Sandstone Formation, BaghGroup of Manawar area, Dhar district, Madhya Pradesh; *J. Geol. Soc. India* **46** 229–243.

Laskar J, Fienga A, Gastineau M and Manche H 2011 La2010: A new orbital solution for the long-term motion of the Earth; *Astron. Astrophys.* **532** A89.

Leszczyński K 2017 The significance of Upper Cretaceous hardgrounds and other discontinuity surfaces for basin-wide correlations, based on drillcore data from boreholes in northern Poland; *Geol. Quart.* **61**.

Lewy Z 1975 The geological history of southern Israel and Sinai during the Coniacian.

Li X, Jenkyns H C, Wang C, Hu X, Chen X, Wei Y, Huang Y and Cui J 2006 Upper Cretaceous carbon- and oxygen-isotope stratigraphy of hemipelagic carbonate facies from southern Tibet, China; *J. Geol. Soc.* **163(2)** 375–382.

Li G, Jiang G and Wan X 2011 The age of the Chuangde Formation in Kangmar, southern Tibet of China: Implications for the origin of Cretaceous oceanic red beds (CORBs) in the northern Tethyan Himalaya; *Sedim. Geol.* **235(1–2)** 111–121.

Liu H, Shi K, Liu B, Song X, Li Guo R Y, Wang G, Wang H and Shen Y 2019 Characterisation and identification of bioturbation-associated high permeability zones in carbonate reservoirs of Upper Cretaceous Khasib Formation, AD oilfield, central Mesopotamian Basin, Iraq; *Mar. Pet. Geol.* **110** 747–767.

Martin-Chivelet J and Giménez R 1992 Paleosols in microtidal carbonate sequences. Sierra de Utiel Formation, Upper Cretaceous, SE Spain; *Sedim. Geol.* **81** 125–145.

Matsumoto T 1973 In: *Late Cretaceous Ammonoidea in Atlas of Paleobiogrography* (ed.) Hallam A, Elsevier Scientific Publishing Company, Amsterdam, pp. 421–429.

Mercey N D E 1872 Sur l'Argile a Silex; *Bull. Soc. Geol. Fr.* I, 3rd Ser., 134–137.

Molenaar N and Zijlstra J J P 1997 Differential early diagenetic low-Mg calcite cementation and rhythmic hardground development in Campanian-Maastrichtian chalk; *Sedim. Geol.* **109(3–4)** 261–281.

Olszewska-Nejbert D 2004 Development of the Turonian/Coniacian hardground boundary in the Cracow Swell area (Wielkanoc quarry, Southern Poland); *Geol. Quart.* **48** 159–170.

Olszewska-Nejbert D and Świerczewska-Gładysz E 2013 Facies and sedimentation of Coniacian deposits of the Kraków Swell in the Wielkanoc area (southern Poland); *Geol. Quart.* **57** 1–16.

Patel S J, Shitole A D and Joseph J K 2018 Plug Shaped Burrows Conichnus-Conostichus from the Late Cretaceous of Bagh Group, Gujarat, Western India; *J. Geol. Soc. India* **91** 41–46.

Piovesan E K, Nicolaidis D D, Fauth G and Viviers C 2013 Ostracodes from the Aptian-Santonian of the Santos, Campos and Espírito Santo basins, Brazil; *J. South Am. Earth Sci.* **48** 240–254.

Piovesan E K, Cabral M C, Colin J P, Fauth G and Trescastro Bergue C 2014a Ostracodes from the Upper Cretaceous deposits of the Potiguar Basin, northeastern Brazil: Taxonomy, paleoecology and paleobiogeography. Part 1: Turonian; *Carnets De Géologie/notebooks on Geology* **14** 211–252.

Piovesan E K, Cabral M C, Colin J P, Fauth G and Trescastro Bergue C 2014b Ostracodes from the Upper Cretaceous deposits of the Potiguar Basin, northeastern Brazil: Taxonomy, paleoecology and paleobiogeography. Part 2: Santonian-Campanian; *Carnets De Géologie/notebooks on Geology* **14** 315–351.

Pollock R E 1976 The depositional environments of the Maastricht and Kunrade Chalks (Maastrichtian) from the type area of Limburg, Netherlands; *Staringia* **3(1)** 16–18.

Pomoni-Papaioannou F 1994 Palaeoenvironmental reconstruction of a condensed hardground-type depositional sequence at the Cretaceous-Tertiary contact in the Parnassus-Ghiona zone, central Greece; *Sedim. Geol.* **93(1–2)** 7–24.

Pomoni-Papaioannou F and Solakius N 1991 Phosphatic hardgrounds and stromatolites from the limestone/shale boundary section at Prossilion (Maastrichtian–Paleocene) in the Parnassus-Ghiona Zone, Central Greece; *Palaeogeogr. Palaeoclimatol. Palaeoecol.* **86(3–4)** 243–254.

Pomoni-Papaioannou F and Zambetakis-Lekkas A 2009 Facies associations of the late Cenomanian carbonate platform of Tripolitza subzone Vitina, Central Peloponnesus, Greece: Evidence of long-term/terrestrial subaerial exposure; *Bull. Soc. Geol. J. Geosci.* **128** 1.

Powell J H and Moh'd B K 2011 Evolution of Cretaceous to Eocene alluvial and carbonate platform sequences in central and south Jordan; *GeoArabia* **16(4)** 29–82.

Puckett T M, Andreu B and Colin J P 2016 The evolution of the Brachycytheride Ostracoda in the context of the breakup of Pangea; *Revue De Micropaléontologie* **59(2)** 97–167.

Rasser M W, Scheibner C and Mutti M 2005 A paleoenvironmental standard section for Early Ilerdian tropical carbonate factories (Corbieres, France; Pyrenees, Spain); *Facies* **51** 217–232.

Reitner J, Wilmsen M and Neuweiler F 1995 Cenomanian/Turonian sponge microbialite deep-water hardground community (Liencres, northern Spain); *Facies* **32(1)** 203–212.

Reuss A E 1845 *Die Versteinerungen der böhmischen Kreide formation. – E. Schweizerbart'sche Verlags-buchhandlung und Druckerei*, 58p.

Richard J, Sizun J P and Machhour L 2005 Environmental and diagenetic records from a new reference section for the Boreal realm: The Campanian chalk of the Mons basin (Belgium); *Sedim. Geol.* **178** 99–111.

Ruidas D K, Paul S and Gangopadhyay T K 2018 A reappraisal of stratigraphy of Bagh Group of rocks in Dhar district Madhya Pradesh with an outline of origin of nodularity of Nodular Limestone Formation; *J. Geol. Soc. India* **92(1)** 19–26.

Ruidas D K, Pomoni-Papaioannou F A, Banerjee S and Gangopadhyay T K 2020 Petrographical and geochemical constraints on carbonate diagenesis in an epeiric platform deposit: Late Cretaceous Bagh Group in central India; *Carbonate Evaporite* **35** 94.

Saller A H and Moore C H Jr 1991 Geochemistry of meteoric calcite cements in some Pleistocene limestones; *Sedimentology* **38(4)** 601–621.

Salomons W, Goudie A and Mook W G 1978 Isotopic composition of calcrete deposits from Europe, Africa and India; *Earth Surf. Process.* **3(1)** 43–57.

Sarkar S K 1973 Sedimentray of the Narmada Bagh Lameta complex around Awaldaman and Bagh areas, Dhar Distrct, Madhya Pradesh; Ph.D thesis, Jadavpur University, 190p.

Scholle P A and Ulmer-Scholle D S 2003 A color guide to the petrography of carbonate rocks: Grains, textures, porosity, diagenesis, *AAPG Memoir* **77(77)**.

Shitole A D, Patel S J, Darngawn J L and Josep J K 2021 Amended lithostratigraphy of the Cretaceous Bagh Group, Western Lower Narmada Valley, India: A comparison with pervasive Tethyan basins; *Geol. J.* **56(10)** 5058–5093.

Singh I B 1981 Palaeoenvironment and palaeogeopraphy of Lameta Group Sediments Late Cretaceous in Jabalpur area, India; *J. Palaeontol. Soc. India* **26** 38–53.

Singh S K and Dayal R M 1979 Trace fossils and environment of deposition of Nimar Sandstone, Bagh Beds; *J. Geol. Soc. India* **20** 234–239.

Singh I B, Shekhar S and Agarwal S C 1983 Palaeoenvironment and stratigraphic position of green sandstone Lameta: Late Cretaceous Jabalpur area; *J. Geol. Soc. India* **24** 412–420.

Skelton P W, Spicer R A, Kelley S P and Gilmour I 2003 *The cretaceous world*; 360p.

Sowerby J D C 1826−1829 *The mineral conchology of Great Britain or coloured figures and descriptions of those remains of testaceous animals or shells, which have been preserved at various times and depths in the earth*; B Meredith, London **6** (1st edn), 230p.

Spence G H and Tucker M E 1997 Genesis of limestone megabreccias and their significance in carbonate sequence stratigraphic models: A review; *Sedim. Geol.* **112(3–4)** 163–193.

Srivastava A K and Mankar S R 2012 Trace fossils and their palaeoenvironmental significance in the Lameta Formation of Salbardi and Belkher area, district Amravati, Maharashtra, India; *Arab. J. Geosci.* **5** 1003–1009.

Taylor P D and Badve R M 1995 A new Cheilostoma bryozoan's genus from the mid-cretaceous of India and Europe and its strong Homeomorphy with cyclostomes; *Palaeontology* **38(3)** 627–658.

Taylor P D and Wilson M A 2003 Palaeoecology and evolution of marine hard substrate communities; *Earth-Sci. Rev.* **62** 1–103.

Tripathi S C 2006 Geology and evolution of the Cretaceous infratrappean basins of Lower Narmada Valley, western India; *J. Geol. Soc. India* **674** 459–468.

Tucker M E and Wright V P 1990 *Carbonate sedimentology*; Blackwell Scientific, Oxford, 482p.

Vinn O and Toom U 2015 Some encrusted hardgrounds from the Ordovician of Estonia (Baltica); *Carnets De Géologie* **15(7)** 63–70.

Vinn O and Wilson M A 2010 Microconchid-dominated hardground association from the late Pridoli (Silurian) of Saaremaa, Estonia; *Palaeontologia Electronica* **2** 13.2.9A.

Viviers M C, Koutsoukos E A M, Silva-Telles A C and Bengtson P 2000 Stratigraphy and biogeographic affinities of the late Aptian-Campanianostracods of the Potiguar and Sergipe basins of northeastern Brazil; *Cret. Res.* **21** 407–455.

Voigt E 1959 Die ökologische Bedeutung der Hartgründe (Hardgrounds) in der oberen Kreide; *Paläontologische Zeitschrift* **33(3)** 129–147.

Walker R G and James N P (eds) 1992 Facies models. Response to sea level change; *Geol. Assoc. Canada*, Ottawa, 409p.

Watkins D K, Shafik S and Shin I C 1998 *Calcareous nannofossils from the Cretaceous of the Deep Ivorian Basin*; University of Nebraska, Lincoln.

Wilmsen M, Berensmeier M, Fürsich F T, Majidifard M R and Schlagintweit F 2018 A Late Cretaceous epeiric carbonate platform: The Haftoman Formation of central Iran; *Facies* **64(2)** 1–24.

Wilson M E J and Evans M J 2002 Sedimentology and diagenesis of tertiary carbonates on the Mangkalihat Peninsula, Borneo: Implications for subsurface reservoir quality; *Mar. Pet. Geol.* **19** 873–900.

Wilson M A and Palmer T J 1992 *Hardgrounds and hardground faunas*; University of Wales, Aberystwyth.

Wright V P 1994 Paleosols in shallow marine carbonate sequences; *Earth-Sci. Rev.* **35** 367–395.

Zijlstra J J P 1995 The sedimentology of chalk; *Lecture Notes in Earth Sciences* **54** 194.

Zijlstra J J P 1997 About the depth of deposition of the Maastrichtian Chalk of the type area; *Ann. Soc. Géol. du Nord.* **T. 5(2éme série)** 207–213.

Corresponding editor: Joydip Mukhopadhyay